Long term coastline monitoring derived from satellite imagery

Hagenaars, Gerben; Luijendijk, Arjen; de Vries, Sierd; de Boer, Wiebe

Publication date
2017

Document Version
Final published version

Published in
Proceedings of Coastal Dynamics 2017

Citation (APA)
Hagenaars, G., Luijendijk, A., de Vries, S., & de Boer, W. (2017). Long term coastline monitoring derived from satellite imagery. In T. Aagaard, R. Deigaard, & D. Fuhrman (Eds.), *Proceedings of Coastal Dynamics 2017: Helsingør, Denmark* (pp. 1551-1562). Article Paper No. 122

Coastal Dynamics 2017
Paper No. 122

LONG TERM COASTLINE MONITORING DERIVED FROM SATELLITE IMAGERY

Gerben Hagenaars[1], Arjen Luijendijk[2], Sierd de Vries[3] and Wiebe de Boer[4]

Abstract

Satellite imagery provides a unique source of data given its spatial and temporal coverage. In this study, a detection algorithm has been developed and tested to automatically determine the satellite derived waterline (SDW). The SDWs have been compared with traditional coastline measurements at two locations along the Dutch coast, where high quality in-situ data is ample available. The findings are that the SDW can be detected with sub pixel precision, with offsets of about 6.5 m in case of Sentinel-2 images. Also for longer time scales, similarities are found between coastline dynamics based on the SDW positions and traditional indicators based on topographic measurements, hence the SDW may serve as a coastal state indicator. This shows that a time series of SDW positions can be used to study coastal dynamics for any coastal stretch to get a first understanding of the coastline evolution in the period of 1984 – present.

Key words: satellite imagery, Google Earth Engine, coastline dynamics, coastal monitoring, positional accuracy, Dutch coast.

1. Introduction

An increasing pressure on coastal areas is observed worldwide. Relative sea level rise induced by climate change causes beaches to erode and coastal areas to retreat. Estimates based on predicted sea level rise show a coastal land loss that may add up to 6.000 – 17.000 km^2 in the 21st century (Hinkel, et al., 2013). At the same time, anthropogenic pressure on coastal zones will increase in the coming years. These conflicting aspects enhance the need to manage coastal zones in a smart way.

The position of the shoreline can be identified as an important source of information in coastal management practice (Boak & Turner, 2005). Definitions of the shoreline vary, but often the mean high water position on a coastal profile is identified and used in coastal management practice. A temporal set of shoreline positions reveals information on coastal evolutions. The shoreline can be identified on for instance aerial imagery or digital elevation maps. In the Netherlands, a monitoring system based on the beach profile is adopted in which the beach volume is transformed into a single representative coastline (the MKL, Momentane Kustlijn Ligging, (Rijkswaterstaat, 2017)). This line is used in for instance policy making on sand nourishments or other mitigation measures performed along the Dutch coast.

Data on for instance the shoreline is required for a thorough understanding of the physical responses of a coastal area. These datasets should have a sufficient resolution in both time and space and often require local measurement campaigns. Since coastal erosion is identified as a global risk and coastal dynamics are observed on different time scales, this data should likewise by available for any coastal area for a sufficient amount of time. This is hardly ever the case since most datasets are limited in time and/or space.

Satellite imagery provides data on a global scale with a frequent revisit time (every 5-16 days) and a moderate spatial resolution (~30 m). Since 1984, satellites from the National Aeronautics and Space Administration (NASA) obtain multispectral data from the earth's surface. More recently, the European Satellite Agency (ESA) launched their Sentinel 2 missions with an even higher resolution (~10 m). Image

[1] Delft University of Technology & Deltares, The Netherlands, gerben.hagenaars@deltares.nl
[2] Delft University of Technology & Deltares, The Netherlands, a.p.luijendijk@tudelft.nl
[3] Delft University of Technology, The Netherlands, sierd.devries@tudelft.nl
[4] Deltares, The Netherlands, wiebe.deboer@deltares.nl

processing techniques are able to make a distinction between pixels containing land (e.g. beaches) from pixels containing water (e.g. seas). The border separating water and land pixels comprises information on the waterline observed along a coastal stretch.

Processing data from satellite images used to be laborious and time-consuming, making it difficult to use satellite data to its full extend. Recently, Google launched the Google Earth Engine (GEE) platform with the purpose of removing the traditional computational limitations in satellite image processing. GEE is a cloud-based platform for the analysis of geospatial data that combines both Google's computational infrastructure and a petabyte archive of publicly available imagery (amongst others NASA Landsat and ESA Sentinel). The combination of cloud storage and parallel cloud computing on the server side of the platform results in a reduction of satellite image processing time from hours to minutes (Google Earth Engine (2015)). The GEE allows for the opportunity to use all available satellite images of NASA and ESA to obtain a historical dataset of global waterline data. An example of which is the recently launched Aqua Monitor (Donchyts, et al., 2016).

The waterline position detected from satellite imagery is assessed in multiple studies (Pardo-Pascual et al. (2012), Garcia-Rubio et al. (2015), Ekercin (2007)), in which the position is found to be closely positioned to in-situ data. However, these studies were often limited by the amount of images used, the spatial extend, the amount of satellite sensors or the quality of the in-situ data. Besides, methods to mitigate traditional sources of inaccuracy such as cloud cover on the waterline quality are not yet assessed. Using the GEE overcomes these limitations, allowing for the opportunity to study all available images from all available sensors.

In this study the Dutch coast bordering the North Sea basin is studied using satellite images for the period 1984 - 2016. The positional accuracy and application range of SDW positions is tested against in-situ measurements for two case studies. A long tradition in measurement campaigns results in ample data availability, with a unique annual topographic dataset conducted since the 1960's (the JarKus, Jaarlijkse Kustlijn meting dataset) and an abundance of data on hydrodynamics. We aim to validate the positional accuracy and revealed long term coastal evolutions of the SDW using the in-situ data quality of this data rich environment. These insights allow for the opportunity to use satellite imagery for coastal areas without much available data, where satellite images may provide the only (historical) source of information.

2. Site description

Coastline dynamics based on both satellite images and in-situ measurements are compared for two coastal stretches along the Dutch coast. The first case study is defined at the coastal stretch near Petten. This area is located at the northern part of the Holland coast. A narrow strip of dunes separates the city of Petten from the beach. This coast has an erosive character that is stabilized in 1880 by means of the Hondschbosche and Pettemer sea defence (HPZ, Hondschbosche and Pettemer Zeewering). The HPZ consists out of multiple groynes and a revetment constructed from asphalt and concrete blocks. Adjacent to the revetment a system of dunes and groynes is present, introducing somewhat more dynamic behaviour to the coastline position. Because this case study comprises both a concrete and a sandy shoreline, insight is obtained in the behaviour of the SDW along these beach characteristics. The area of interest is formed by both the revetment near Petten and the adjacent coast, comprising a coastal stretch of 15.5 km in total. In 2014 a nourishment was put into place in front of the revetment, restoring the original sandy foreshore and dunes. The Petten case is studied for the period 01-01-1984 to 01-07-2016. The case study site and the relevant JarKus transects are indicated in the top panel of Figure 1.The second case study is defined at the coast of Ameland, which is one of the Dutch Waddensea islands located in the north. This island comprises both a sandy shoreline at the North Sea (northern) and a muddy coast at the Waddensea (southern) part of the island. The island is rather dynamic with periods of erosion and accretion at the eastern end of the island. At the western end of the island, a shoal called the Bornrif attached to the coast in the past decades, extending the beach seaward. The North Sea (sandy) coast of the island is studied for the period 01-01-1984 to 01-07-2016. This case study is more dynamic compared to the static revetment and dunes near Petten, and hence provides insight into the applicability of coastline dynamics based on satellite images for dynamic sandy locations. The Ameland case study is indicated in the bottom panel of Figure 1.

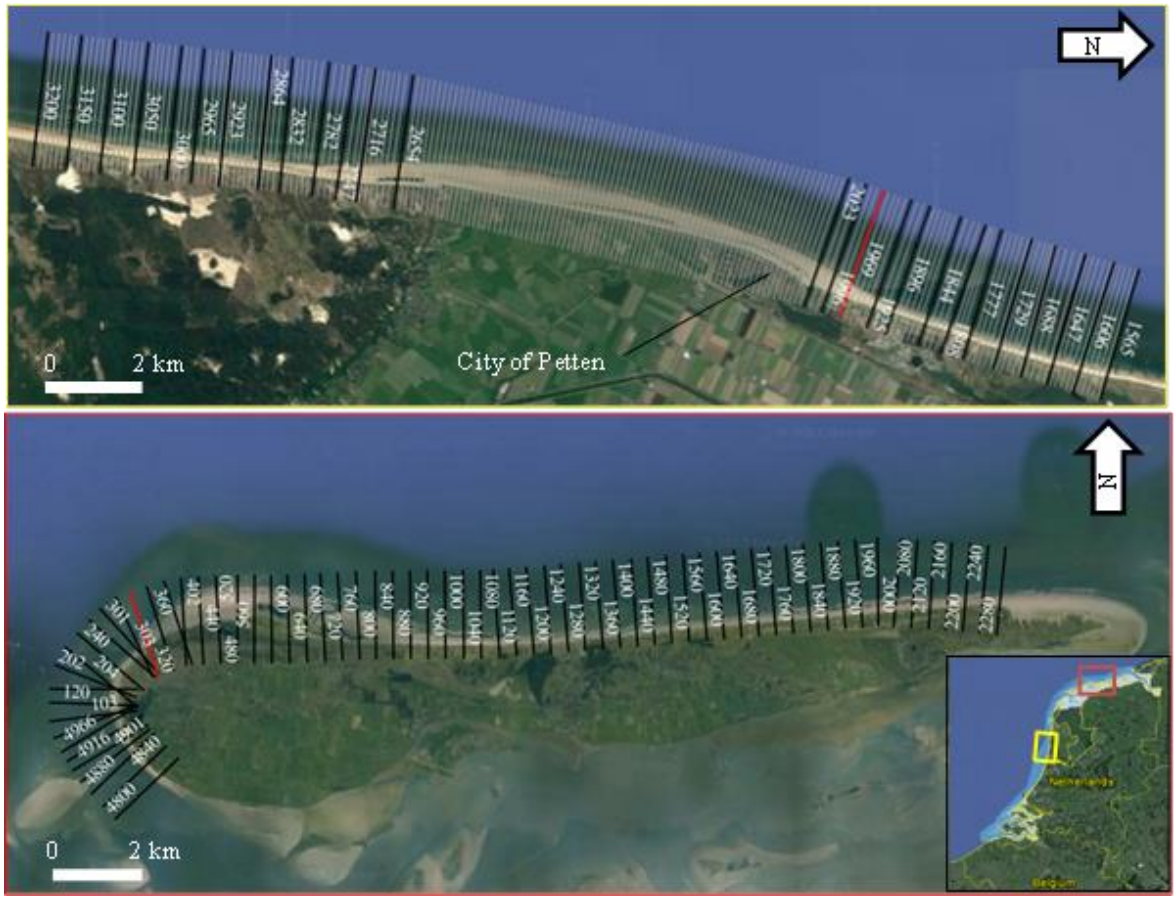

Figure 1 Petten (yellow) and Ameland (red) case study sites. For Petten both the JarKus transects (black) and the refined transects (grey) are indicated. For Ameland only the JarKus transects are indicated. Transects 1983 and 320 are plotted in red.

3. Data availability

The optical satellite imagery is provided by NASA and ESA and is available on the GEE platform. All available Landsat 5, 7 and 8 images are used for both study sites. Table 1 provides an overview of the amount of images and properties per satellite mission. Since both study sites are located on a different image path and row footprint, the amount of images varies for both locations. The radiance values detected on the sensors are transformed to Top-Of-Atmosphere (TOA) radiance values and corrected to a L1T product (meaning that both geometric and radiometric corrections are performed) by the GEE platform. Georeferencing of the image pixel locations is performed with respect to the first image in the collection.

Table 1 Overview of the amount of images and the spatial and temporal characteristics of the different satellite missions.

Satellite mission	Number of images		Spatial resolution [m]	Revisit time [days]
	Petten	Ameland		
Landsat 5	165	267	30 x 30	24
Landsat 7	226	373	30 x 30	16
Landsat 8	101	146	30 x 30	8
Sentinel 2	14	16	10 x 10	5

Both Petten and Ameland are part of the national annual coastline monitoring campaign JarKus provided by the Dutch ministry of public works (Rijkswaterstaat). The beach topography is measured

every 1 – 2 m along cross shore transects that are defined more or less perpendicular to the coastline. These cross shore transects are spaced alongshore by approximately 200 m. For the entire analysis period an annual measurement is available along all transects located within the study areas of both cases (54 transects in case of Petten and 135 transects in case of Ameland), as indicated in Figure 1.

Because the HPZ has a static character, historical elevations are not included in the JarKus dataset. Elevations of the HPZ are obtained from the Actueel Hoogtebestand Nederland (AHN) topographic survey. This survey is conducted by means of airborne LIDAR (Laser Imaging Detection and Ranging) instruments. The AHN-data is available for the entire country and is conducted once every 5 - 7 years. Because the HPZ is assumed static in time, only the AHN2 (and not its predecessor AHN1) data is used. This data was acquired in the first quarter of 2011 and has a spatial resolution of about 5 m. During data acquisition, the water level near Petten was -0.5 m NAP. Due to the nature of the LIDAR instruments, information below this water level is not recorded. Elevations from the AHN2 are merged with the yearly JarKus data to obtain a continuous yearly topographic survey for the Petten case study.

4. Methodology

The methodology consists out of three steps: 1) extraction of waterline positions, 2) accuracy (offset) calculation and 3) assessment of coastal evolutions.

4.1 Waterline extraction

The waterline position is extracted using an automatic, unsupervised thresholding algorithm. Based on the radiance value in the Green and Near-InfraRed (NIR) band, the Normalized Difference Water Index (NDWI) value per pixel (following the approach in for instance Liu, Trinder, & Turner (2017)) is calculated using:

$$NDWI = \frac{\lambda_{NIR} - \lambda_{GREEN}}{\lambda_{NIR} + \lambda_{GREEN}} \tag{0.1}$$

in which λ_{NIR} indicates the TOA radiance value in the Near-InfraRed and λ_{GREEN} the TOA radiance value in the Green band per pixel.

Using the classification approach introduced by Otsu (1979), an automatic threshold value is calculated to classify the NDWI values into water and land pixels. Using a region growing algorithm this binary land-water image is clustered into distinct water and land regions. The edge of the water regions are extracted and results in a vector that defines the water-land boundary. This line is referred to as the satellite derived waterline (SDW). A SDW position is extracted from all satellite images described in Table 1. Besides SDW positions from single images, an image composite technique as described in Donchyts, et al. (2016) with a moving average window of 360 days is used to reduce the effects of potential sources of inaccuracy, such as cloud cover. This technique calculates a reduced image based on the 15^{th} percentile value of all satellite image pixel values within the averaging window on a pixel location. All extracted SDW positions are additionally georeferenced by means of 6 manually identified control points in the vicinity of the study sites.

To quantify the positional accuracy of the SDW, a ground truth position of the waterline is recalculated based on the point of intersection of the surveyed topography and the instantaneous water level present during image acquisition. The JarKus transects are spaced alongshore by about 200 m. This is too coarse compared to the image pixel resolution of 30 or 10 m. A refined system of transects with an alongshore spacing of 40 m is therefore defined parallel to the JarKus transects. Per transect, a local water level is obtained based on water level measurements (including both the tide and surges), measured in the vicinity of the coast. The JarKus topography is interpolated towards these transects and the point of intersection is obtained. This set of intersection points results in the position of the survey waterline, that is marked as the ground truth position of the waterline that was present during satellite image acquisition.

4.2 Accuracy calculation

The positional accuracy of the SDW is quantified for the Petten case study by means of the refined cross shore transect system. The accuracy of the SDW position is calculated by means of the horizontal distance between both the SDW and the survey waterline per transect.

Theoretically several sources can be identified that cause deviations in the SDW position. To prevent these sources from effecting the offset calculation, the offset calculation is performed for a single satellite image on which no clouds are detected, no waves are present and for which a JarKus topographic survey was conducted close to satellite image acquisition. This scenario is referred to as the benchmark case. In case of the image composite technique, the reduced SDW position is compared to the survey waterline based on the closest topographic survey and the average water level recorded during image acquisition of all underlying satellite images.

4.3 Coastal evolutions

To study coastal evolutions, the point of intersection between the transect and a time series of subsequent SDW positions is obtained. The distance between the transect origin (located at the landward side of the transect) and the point of intersection is stored for all SDW positions and all transects. Since the transect orientations are fixed in time, this projected distance reveals information about the beach profile width in time, which can be used as a coastal state indicator. To prevent deviations caused by cloud cover, only the 360 days image composites are used in this analysis. To compare trends in this position and to explorer the relation between SDW positions and coastal monitoring practice, the MKL position from the topographic survey is extracted per transect. The MKL is calculated according to the method described in Rijkswaterstaat (2017). This method calculates a weighted average position based on the cross shore elevations located between the dune foot (defined as +3 m NAP) and an elevation below the low waterline. The MKL position reflects the most active profile of the beach profile. Linear regression is applied on the obtained time series, in which the fitted slope is used to quantify the long term trend. Trends obtained from both dataset are compared for the Petten and Ameland case studies.

5. Results

5.1 Positional accuracy

5.1.1 Benchmark case

Figure 2. Landsat 5 image acquired on 16-06-1986. The SDW position is indicated in black.

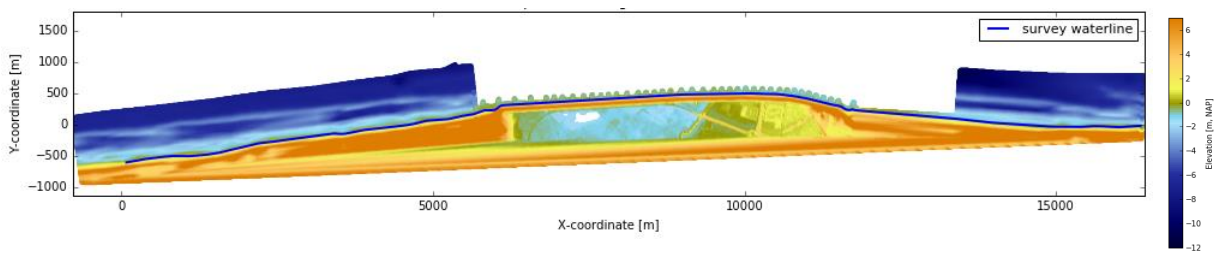

Figure 3 Combined topography of the JarKus and AHN2 dataset. The survey waterline is indicated in blue.

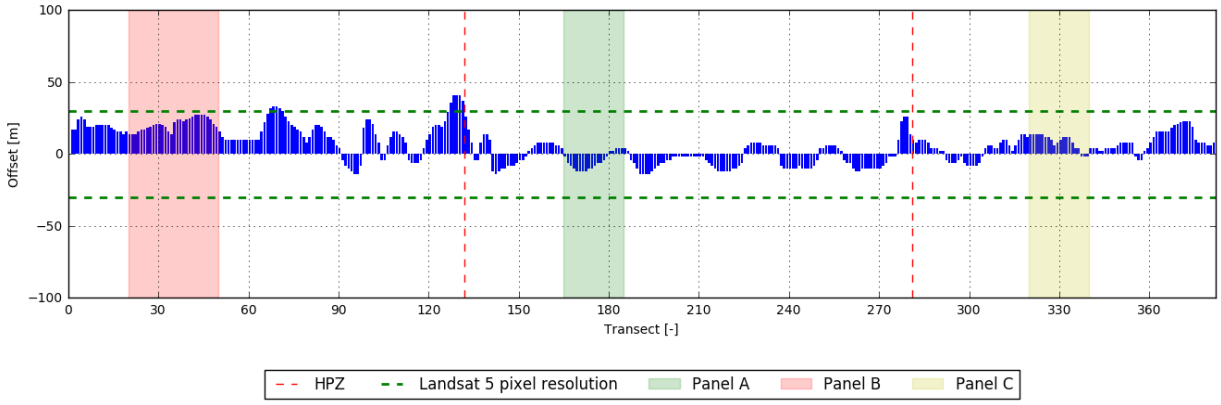

Figure 4 Offset value per transect between the SDW and survey waterline. 3 locations along the coast are indicated.

The Landsat 5 image acquired on 16-06-1986 has a zero detected cloud cover near the location of the waterline. A low offshore wave height of 0.63 m in offshore direction was recorded by the offshore wave platform, indicating that offshore waves are not present on the image. The presence of foam induced by breaking waves cannot be observed by means of visual inspection. This indicates that a highly accurate SDW position can be detected since the main drivers that cause deviations are absent. Figure 2 displays the detected SDW position on this Landsat 5 image.

The JarKus topographic survey was conducted about 3 - 10 days prior to image acquisition, indicating that morphological changes are limited and hence an accurate survey waterline can be reconstructed. The observed water level ranged from + 0.69 m NAP at the southern to + 0.60 m NAP at the northern end of the study site. The survey waterline based on the interpolated topography and measured water level is displayed in Figure 3. All data in the AHN2 dataset that is below the water level present during data acquisition is masked.

The resulting offset between the survey waterline and the SDW is displayed in Figure 4. The transition between the HPZ and the adjacent coast is indicated with a red line, the Landsat 5 image pixel resolution of 30 m is indicated by means of a green horizontal line. A distinction is made between a seaward (the SDW is positioned seaward of the survey waterline) and a landward offset. The first is plotted as a positive and the latter as a negative offset value. A spatial mean offset value of 6.5 m with a standard deviation of 11.6 m is found for the entire domain.

The offset values are almost all below the image pixel resolution of 30 m, indicating that the correct edge of the pixel is found in detecting the SDW. A local zoom-in of three locations (indicated as panels in Figure 4) are displayed in Figure 5. The offset values within the HPZ area show a distinct fluctuation with length scales of about 25 transects (~1.0 km). They weakly relate to the presence of the groynes in front of the revetment, which are spaced by approximately 300 m. Some groynes are not captured well by the AHN2 dataset, and some are not captured well by the SDW, resulting in offset fluctuations. The largest offset values of about the pixel resolution are found in the southern part of the study area. Based on the local zoom in (Panel B), the JarKus topography is shifted landward by about one pixel, which indicates that the topography is more dynamic than close to the static HPZ, and morphologic changes in the time between conducting the survey and image acquisition results in a seaward shift of the waterline. Near the transition between the AHN2 and JarKus datasets (Panel C), offset values of about the pixel resolution are present. At that transition, some transects that are not positioned in the HPZ domain are still represented by the static AHN2 dataset, and hence morphological changes cause inaccuracies in the survey waterline.

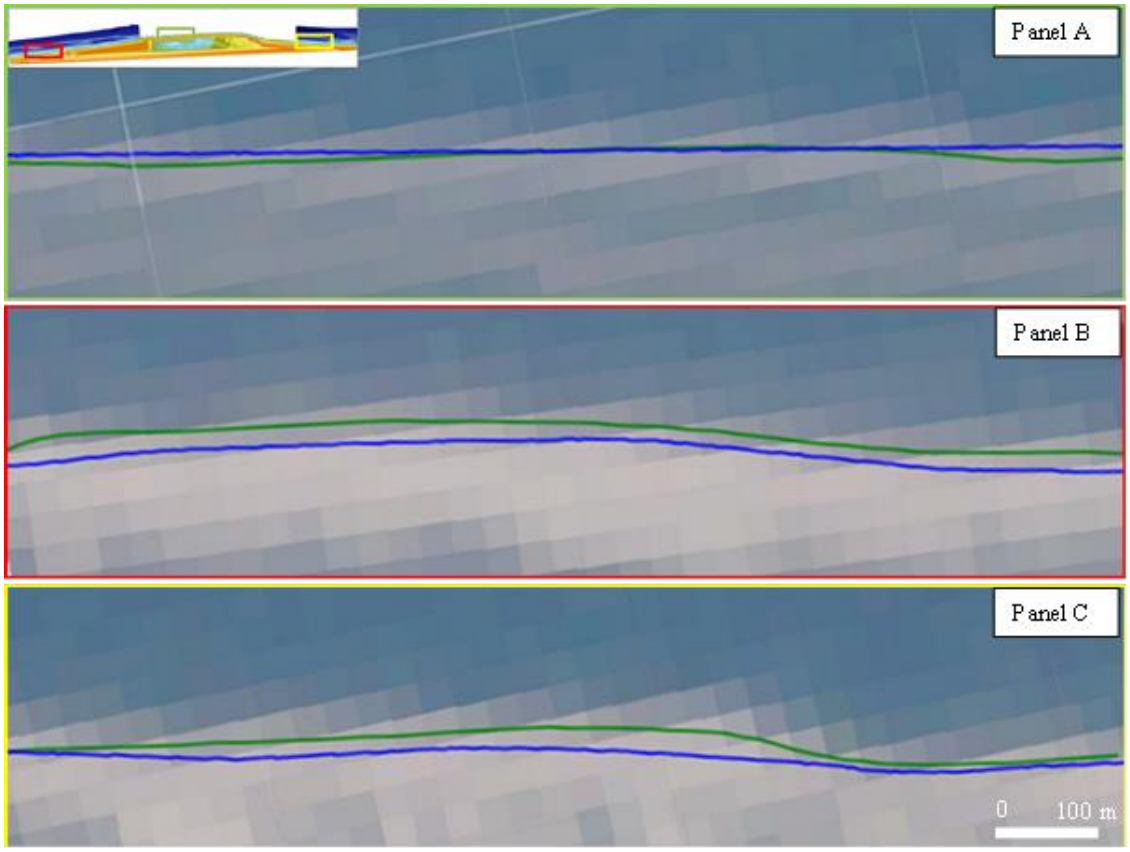

Figure 5 Zoom-ins of the detected SDW position (green) and the survey waterline (blue) for the benchmark case.

5.1.2 Image composites

Sources related to the satellite environment (e.g. cloud cover), satellite instrument and the way the survey waterline is reconstructed (e.g. morphological changes, local water level deviations) can cause the SDW position to deviate from the actual waterline. A moving average image composite window of 360 days is used based on all available satellite images to mitigate these deviations. Figure 6 displays the result of the offset calculation of all individual images and all image composites per transects. Both the average offset, the 95% confidence interval based on a student-T distribution in combination with the standard deviation of the mean per transect and the offset found in the benchmark case are plotted.

In case of all individual images (top panel), large offsets of multiple pixels are present. The large confidence interval indicates that the offset varies over the images. The spatial and temporal averaged offset is 69 m with a standard deviation of 187 m. In case of the image composites (lower panel), the average offset reduces to -10 m with a standard deviation of 19 m. The correct pixel edge is found in detecting the SDW, which results in smaller offsets than present for the benchmark case. This is most pronounced in the more dynamic JarKus domain of the study area . The confidence interval is small, indicating that the offset is about constant for all images along all transects.

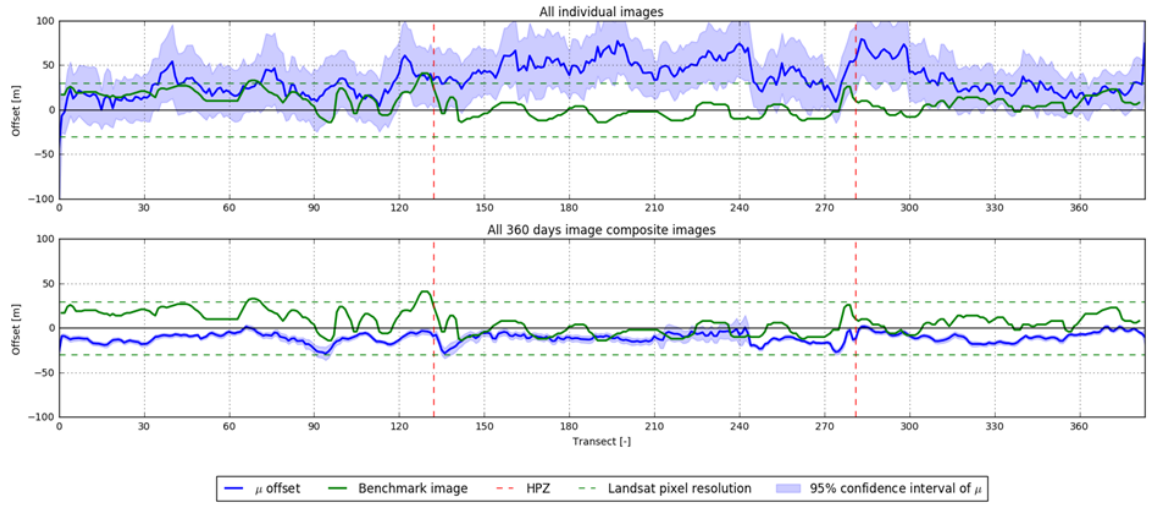

Figure 6 Offset distribution for all transects in case of all individual images (top panel) and all 360 days image composite images (bottom panel). The offset value found for the benchmark case is indicated in green, the HPZ domain is indicated in red.

5.2 Coastal evolutions

For both the Petten and Ameland case studies a time series of SDW positions obtained from a 360 days image composite window is studied. A time series is analysed for both study sites.

5.2.1 Petten

Figure 7 Time-lapse of the SDW position detected on a composite image of 1986 (left panel), 2014 (middle panel) and 2016 (right panel).

The coastal evolution of Petten is illustrated in Figure 7. Since the HPZ is static, and the adjacent coast is maintained stable, the SDW shifts with a maximum of only 1 pixel between concurrent images in the period 1985 – 2014 on some locations. Especially the SDW directly attached to the HPZ may shift seaward and landward in time. The groynes are sometimes included in the SDW, but the static behaviour of this coastal stretch is clearly represented by the images. Both the nourishment construction in 2014 and the present state of the beach in 2016 are captured in the SDW position, as indicated in the second and third panel of Figure 7.

The SDW positions obtained from the 360 days composite window are intersected with the system of transects to obtain a timeseries of the distance between the SDW location and the transect origin. The resulting timeseries for transect 1983 is plotted in Figure 8. The location of transect 1983 is indicated in red in the top panel of Figure 1. The MKL position is obtained for this transect based on the JarKus elevation profiles. This position is used in the Netherlands to assess whether a nourishment mitigation measure is required for this location. Due to its defintion, the MKL position is located on a more elevated position compared to the SDW. Therefore the SDW position is shifted by the difference between the average value of the MKL distance and SDW distance with respect to the transect origin. This results in a landward shift of 500 m for this specific transect. The timeseries of the MKL position is indicated in blue in Figure 8. Since this location is rather static, both the MKL and SDW positions show small fluctuations of only 1 or 2 pixels, indicating that a shift in pixel edges is observed. In 2000 the SDW positions shift

seaward with multiple pixes. This flucatuation is not captued in the MKL position. The MKL and SDW show similarities in shifts and behavior.

Linear regression is performed on the timeseries, of which the resulting fit is plotted in Figure 8 for both datasets. Both the SDW and MKL positions result in a positive trend, indicating local accretion of 1.1 m/year based on the SDW and 1.2 m/year based on the MKL. A RMSE of 0.1 m/year is found when comparing the fitted trends of the SDW and MKL dataset on all JarKus transects. Because measured coastal elevations near the HPZ are not publicly available, the comparision is anly performed for the period of 1984 – 2014.

Figure 9 displays the spatial pattern of the fitted change rate of all SDW positions per transect. Accretion is observed over all transects, except for the transect directly adjacent to the HPZ. The seaward trend is limited to about 1-2 m/year, indicating that this coastal stretch is rather static.

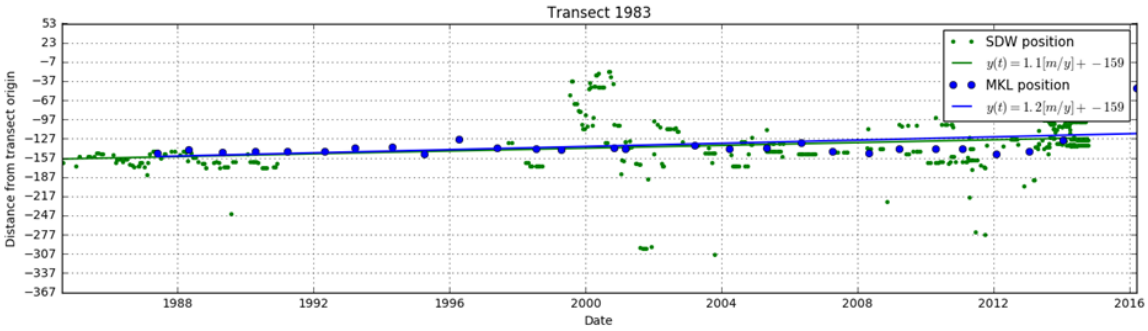

Figure 8 Time series of SDW positions (green) and MKL positions (black) projected along transect 1983. The resulting linear fit for both datasets is indicated in green and blue.

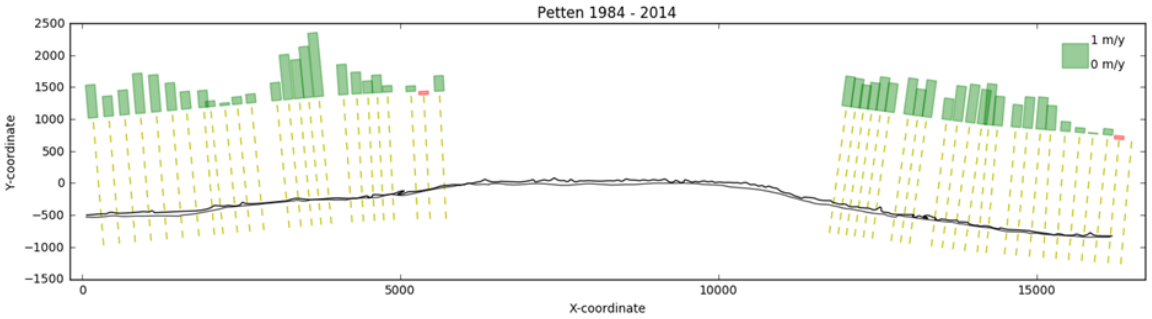

Figure 9 Spatial overview of the rate of change obtained from the linear fit through the SDW positions for all JarKus transects in the Petten case study domain. An seaward (accretion) trend is indicated in green and an erosive (landward) trend is indicated in red.

5.2.2 Ameland

For Ameland all 360 day image composite SDW positions are detected from the satellite images listed in Table
1. Figure 10 provides a time-lapse of four time instances of the coastal evolution of Ameland. West of the island the migration of the Bornrif shoal is clearly visible in the images. In 1986 this shoal is not yet detected in the SDW position since a channel separates the shoal from the coastline. In 2015 the shoal is further attached to the island and in the 2006 situation, the Bornrif is attached to the coastline and fully included in the SDW. On the eastern end of the island migrating shoals are sometimes included in the SDW, depending on the local soil wetness. This tip is not always detected well by the SDW since increased soil wetness can cause NDWI values in the range of water. On the Waddensea side of the island, the SDW position is effected by the local soil wetness of the muddy coast present, resulting in local seaward deviations of the SDW.

The SDW position is intersected with the system of transects to obtain a timeseries of the distance between the SDW location and the transect origin. The resulting time series for transect 320 is plotted in Figure 11. The location of transect 320 is indicated in red in the bottom panel of Figure 1. The MKL

position is obtained for this transect based on the JarKus elevation profiles, and plotted in blue in Figure 11. To allign the SDW and MKL, a landward shift of 500 m for all SDW distances is applied for this transect. Only the period of 2006 – 2017 is plotted.

The resulting timeseries show similarities between the MKL and SDW positions. Seaward shifts in 2012 and 2016 are captured both by the SDW and MKL. A landward shift of about 30 m is visible for both datasets in the period 2012 – 2016 (distances going from 329 m to 209 m).

Figure 10. Time-lapse of the SDW position detected on a composite image of 1986 (upper left panel), 1999 (upper right panel) 2006 (lower left panel) and 2015 (lower right panel).

A linear relation is fitted through both the SDW and MKL positions, of which the slope reveals information about the structural rate of coastline change. The resulting fits for transect 320 are plotted in Figure 11. In case of the SDW positions, a changerate of -4.7 m/year is found, which is -3.8 m/year in case of the MKL positions. The changerates of the SDW and MKL positions compare well, and a RMSE over all JarKus transects of 6.9 m/year is found. Especially near the attachtment of the Bornrif (near transect 640), the changerates starts to deviate significanlty. This is mainly due to the definition of the MKL, which is set constant in this period and the sudden step in SDW positions due to the attachment of the shoal. When these transects are filtered out of the analysis, a RMSE of 1.9 m/year is found when comparing the MKL and SDW changerates for the remaining transects.

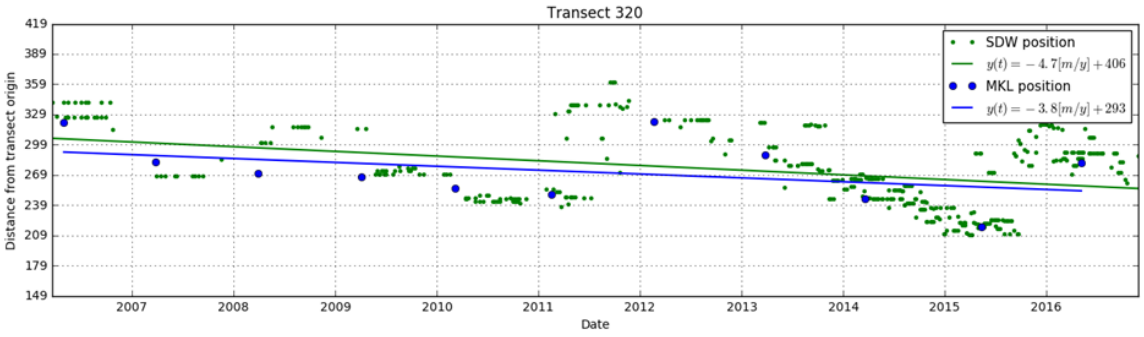

Figure 11. Time series of SDW positions (green) and MKL positions (black) projected along transect 320. The resulting linear fit for both datasets is indicated in green and blue.

Performing the linear fit for all transects defined along the Ameland North sea coasts results in the coastal evolution patterns as indicated in Figure 12. The attachtment of the Bornrif shoal is clearly visible in this figure, with an accretion of more than 10 m/year. The western tip of the island is affected by an errosive trend of more than 10 m/year. Along the eastern part of the island the rate of change indicates less dynamic behavior with changerates of about 1 – 2 m/year.

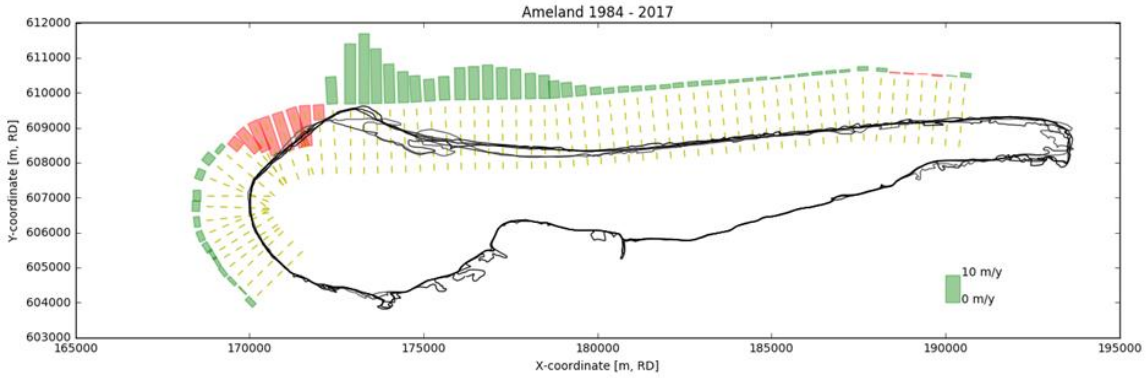

Figure 12 Spatial overview of the rate of change obtained from the linear fit through the SDW positions for all JarKus transects in the Ameland case study domain. A seaward (accretion) trend is indicated in green and an erosive (landward) trend is indicated in red

6. Discussion

Both a muddy and a sandy coast are present for the Ameland case study. The SDW position along the sandy shore is able to follow the waterline, except for the eastern tip of the island where increased soil wetness might induce deviations. Along the muddy coast, seaward deviations are sometimes detected in case of wet soils present during low water. The transition between land and water is less distinct, and a single land-water classification threshold value is not sufficient. This is also partly affected by the distinct sand-water transition, which shifts the optimal unsupervised threshold value. The classification miss match might change when the sandy and muddy shores are treated separately by calculating a single sandy and muddy unsupervised threshold value instead of a single value for the entire domain.

Satellite imagery provides 1D information on the coast, while the MKL includes 2D (volume) information. SDW positions therefore lack the ability to provide information on beach volumes, which are essentially required to study the safety level of a coastal area. For instance seasonal fluctuations in beach slope cause deviations in the waterline that does not necessary indicates a decrease in beach volume. Because of the annual time scale of the JarKus data, the MKL position was adopted in the Netherlands to compensate for these inter-annual fluctuations. However, this study shows that trends in SDW positions can serve as an indicator of the MKL position, which is based on beach volume. Since the waterline is a proxy of this volume, shifts in SDW positions relate to shifts of the entire beach profile.

Since the launch of the Sentinel 2 satellite in 2015, the Landsat 7, 8 and Sentinel 2 missions are all operational, resulting in a frequent revisit time. For the Dutch coast this means that 11 – 14 images are available per month. Since this may result in more cloud free satellite images per month, a combination of all these sensors results in coastal features that can be studied on smaller timescales. Because of this higher temporal frequency, the actual state of the shoreline might be better represented by means of the inter-annual temporal satellite image frequency compared to the annual MKL information. Besides, an increasing spectral and spatial resolution is expected in the near future with the introduction of new satellite missions. This makes it possible to detect more features on satellite images and to study coastal features on smaller spatial scales.

7. Findings

The SDW detection algorithm is able to extract waterline locations in an unsupervised way from optical satellite imagery. Based on the Petten case study the average offset of this waterline is 6.5 m when compared to highly accurate, recent data on the in-situ waterline. Due to the static behaviour of the HPZ, small offsets are found even though this topography was acquired in 29 year after acquisition of the benchmark image. This average offset indicates that the correct pixel edge separating land and water is found and that offsets on a sub pixel level are obtained. Using a moving average image composite technique with a window of 360 days results in offset values below the pixel resolution for all available images. This techniques results in a continuous dataset of which the offset is about constant for all images.

Large scale coastal evolutions, such as the Petten nourishment or the attachment of the Bornrif shoal to the coastline are captured by the SDW. In case of increased soil wetness (such as along the Waddensea coast of Ameland) or along locations with migrating shoals and channels (such as at the eastern tip of Ameland), the SDW fluctuates and may shift landward due to similarities in NDWI values between the wet soils and water.

Change rates obtained from a time series of SDW and MKL positions show similarities in both trend direction and magnitude. A RMSE of 0.4 m/year is found in case of Petten and 1.9 m/year in case of Ameland. Because of the rather dynamic behaviour of the Ameland case study the change rates start to deviate. The attachment of the Bornrif shoal results in differences in the MKL and SDW due to differences in definitions.

SDW positions provide a unique dataset that is able to follow coastal evolutions and relates to traditional coastal indicators. Performing the algorithm on the GEE platform results in run times of about 1 – 2 days per case for all available Landsat and Sentinel images. Due to the nature of satellite imagery, the SDW can be used for any location in the world to obtain a historical coastal indicator for the period of 1984 – present.

References

Boak, E. H., & Turner, I. L. (2005). Shoreline Defintion and Detection: A Review. *Journal of Coastal Research 21(4)*, 688-703.

Donchyts, G., Baart, F., Winsemius, H., Gorelick, N., Kwadijk, J., & van de Giesen, N. (2016). Earth's surface water change over the past 30 years. *Nature Climate Change* (pp. 810–813). NATURE CLIMATE CHANGE.

Ekercin, S. (2007). Coastline Change Assessment at the Aegean Sea Coasts in Turkey using multitemporal Landsat Imagery. *Journal of Coastal Research*, 691-698.

Garcia-Rubio, G., Huntley, D., & Russell, P. (2015). Evaluating shoreline identification using optical satellite images. *Marine Geology*, 96-105.

Google Earth Engine Team. (2015, 12). Google Earth Engine: A planetary-scale geo-spatial analysis platform.

Hinkel, J., Nicholls, R., Tol, R., Wang, Z., Hamilton, J., Boot, G., . . . Klein, R. (2013). A global analysis of erosion of sandy beaches and sea-level rise: An application of DIVA. *Global and Planetary Change* (pp. 150-158). Elsevier.

Liu, Q., Trinder, J., & Turner, I. L. (2017). Automatic super-resolution shoreline change monitoring using Landsat archival data. *Journal of Applied Remote Sensing*.

Otsu, N. (1979). A Threshold Selection Method from Gray-Level Histograms. *IEEE Transactions on systems, man and cubernetics*.

Pardo-Pascual, J. E., Almonacid-Caballer, J., Ruiz, L. A., & Palomar-Vazquez, J. (2012). Automatic extraction of shorelines from Landsat TM and ETM+ multi-temporal images with subpixel precision. *Remote sensing of the Environment*, 1-11.

Rijkswaterstaat. (2017). *Kustlijnenkaarten 2017*. Netherlands: Rijkswaterstaat.